Determination of magnetic parameters in La0.7Sr0.3MnO3/SrTiO3 thin films using EMCD

Gen Li, Dongsheng Song, Zhi Peng Li, and Jing Zhu

Citation: Applied Physics Letters **108**, 242414 (2016); doi: 10.1063/1.4954168
View online: http://dx.doi.org/10.1063/1.4954168
View Table of Contents: http://scitation.aip.org/content/aip/journal/apl/108/24?ver=pdfcov
Published by the AIP Publishing

Determination of magnetic parameters in $La_{0.7}Sr_{0.3}MnO_3/SrTiO_3$ thin films using EMCD

Gen Li, Dongsheng Song, Zhi Peng Li, and Jing Zhu[a)]
National Center for Electron Microscopy in Beijing, Key Laboratory of Advanced Materials (MOE) and the State Key Laboratory of New Ceramics and Fine Processing, School of Materials Science and Engineering, Tsinghua University, Beijing 100084, People's Republic of China

(Received 31 March 2016; accepted 4 June 2016; published online 15 June 2016)

It is well known that the magnetic state of the $La_{0.7}Sr_{0.3}MnO_3$ (LSMO) thin-film heterostructure is strongly correlated with the lattice, spin, orbital, and charge states, since these influence the electric and magnetic transport properties even on the unit-cell level. Therefore, understanding the material's magnetic properties on the nanoscale is important for the development of novel applications. The recently developed electron magnetic-circular dichroism (EMCD) technique allows the determination of atomic site-specific magnetic information via the use of transmitted electrons; however, its sensitivity is not high enough to quantitatively acquire magnetic information in many weak magnetism systems. Here, we utilized a dynamical diffraction-effect assisted EMCD technique to quantitatively determine the spin and orbital magnetic moment of LSMO/$SrTiO_3$ thin films on the nanometer scale using a transmission electron microscope. Further, data processing was optimized to enhance the intensity of the EMCD signals for manganese, which have very weak magnetism at room temperature. High signal-to-noise ratio and accurate quantitative magnetic measurement are eventually achieved. Finally, the spin magnetic moments ($0.73 \pm 0.26\,\mu_B$) are derived, and we also limited the ratio of the orbital to spin magnetic moment within an interval of (-0.03, 0.01). Our results not only present the nanoscale magnetic parameters of LSMO/$SrTiO_3$, but also demonstrate how the measurement limit of the spin (or orbital) magnetic moment can be achieved, which is via the developed dynamical diffraction effect assisted EMCD technique. *Published by AIP Publishing.* [http://dx.doi.org/10.1063/1.4954168]

Because of their high spin-polarization ratio near the Fermi surface and semi-metal properties,[1] epitaxial $La_{0.7}Sr_{0.3}MnO_3$ (LSMO) layers are often incorporated in technologically important spintronics devices, such as spin valves, spin injectors, or multiferroic tunnel junctions.[2] The valence of manganese ions can be either trivalent or tetravalent and exhibit double exchange interactions in the form of Mn-O-Mn with the help of oxygen anions, which induce the ferromagnetism with a high Curie temperature up to 370 K.[3,4] Particularly, the magnetism of LSMO is closely related to its chemical bonds; hence, it is speculated that the magnetization states differ in various zones of the thin films. However, traditional magnetic analysis methods, such as superconducting quantum interference device or vibrating sample magnetometer can only provide the magnetic properties in bulk; and although measurements with surface sensitivities on the scale of 5 nm can be obtained via X-ray magnetic circular dichroism, its lateral resolution is still on the sub-micron scale.

Fortunately, the recently developed electron magnetic-circular dichroism (EMCD) technique[5] allows us to characterize magnetism on the nanoscale via high spatial resolution transmission electron microscopy (TEM). Using a specific two-beam or three-beam diffraction geometry, two electron energy loss spectra (EELS) are acquired at the pre-defined "positive" and "negative" symmetric positions in the diffraction plane. The EMCD signal is the difference of these two spectra. The use of sum rules makes it possible to quantitatively obtain magnetic parameters directly from the EMCD signals;[6] the application of various signal collection modes[7–10] has already greatly increased the spatial resolution of EMCD technique to 2 nm. In 2013, researchers in Zhu's group combined the atom location by channeling-enhanced microanalysis method and EMCD technique, and then developed the site-specific EMCD technique, which allows the quantitative determination of atomic site-specific magnetic information with the use of transmitted electrons.[11] Later, researchers further analyzed the influence of the geometry's asymmetry on the distribution of signals,[12] broke the limit of crystal structure in site-specific EMCD experiments,[13] and achieved a simultaneous measurement of the lattice constants, valences of the elements, and magnetic parameters.[14]

In the past few years, the EMCD technique has mainly been utilized in research involving magnetic elements such as Fe, Co, and Ni, because the magnetic moments of these elements, their alloys,[5–9,15,16] or their compounds[10–14,17] are relatively high. Nonetheless, there are few investigations involving manganese. Rubino *et al*. discussed the manganese EMCD signals of $Pr_{0.5}Sr_{0.5}MnO_3$ at various temperatures and found that only the one within the ferromagnetic phase temperature range presented a clear L3 edge;[18] Schattschneider *et al*. showed the EMCD signals of Mn and Co in the Heusler alloy Co_2MnSi;[19] Ennen *et al*. acquired EMCD signals of Mn and Ni in the Heusler alloy Ni_2MnSn (both contained strong background noise and the L2 edges were not clear);[20] and recently Fu *et al*. studied hexagonal MnAs and determined the

[a)]Author to whom correspondence should be addressed. Electronic mail: jzhu@mail.tsinghua.edu.cn

orbit-spin magnetic moments ratio as 0.07 ± 0.05 via sum rules.[21] Note that there was strong background noise in their EELS, and, as just discussed, many spectra only presented clear L3 edges (their L2 edges were weak or even submerged in the background noise). Moreover, the above work did not give quantitative values of the manganese magnetic moments. There are two main reasons for this.

First, the pre-edge exponential backgrounds should be deducted, and the "positive" and "negative" spectra in the post-edge region need to be normalized before the final differential signal, i.e., the EMCD signal, is attained. The common energy loss edges of Fe, Mn, and O are located at 708 eV, 640 eV, and 532 eV, respectively; therefore, the pre-edge background could be accurately deducted owing to the wider interval between the Fe $L_{2,3}$-edges and O K-edge, while for manganese compounds, the accuracy of the pre-edge background subtraction is reduced since oxygen has a wide spread energy range after its K-edge.

Second, manganese magnetic signals in LSMO are very weak at room temperature. The relationship between magnetic properties and temperature has been systematically investigated in LSMO thin films with different thicknesses; literature data show that the magnetization declines as the thickness of thin films is decreased.[22,23] Further, the manganese magnetic moment value at room temperature is only 20%–40% of that near 0 K;[22–28] hence, the manganese EMCD signals will probably be submerged in statistical errors of the EELS. Besides, some non-magnetic atoms or ions may possess induced small magnetic moments when the electronic structure of the crystal changes.[29] If the sensitivity of EMCD could be further improved to quantitatively acquire weaker magnetic signals, its applications would be greatly expanded.

In this paper, we utilize EMCD to quantitatively determine the magnetic parameters of LSMO/$SrTiO_3$ (STO) thin films on the nanometer scale using TEM. The dynamical diffraction effect is fully utilized, and data processing is optimized to enhance the intensity of the EMCD signals so that the weak magnetism of manganese at room temperature can be probed. A high signal-noise ratio (SNR) and accurate quantitative magnetic measurements were achieved.

LSMO thin films were deposited via pulsed-laser deposition.[30] A Rigaku-H2500 diffractometer with prepositional Kα1-monochromator was used for the X-ray diffraction analysis, and the macroscopic magnetic measurements were made via a superconducting quantum-interference device vibrating-sample magnetometer produced by Quantum Design Company. It can be seen that the LSMO (002) peak lies to the right side of the STO (002) peak by about 1° (Fig. 1(a)), and the sharp peaks reflect good epitaxial growth of the thin film. Further calculations show that the (001) interplanar spacing is 3.844 Å (3.87 Å for the bulk), indicating the existence of in-plane tensile strain. The M-H curve in Fig. 1(b) shows the typical ferromagnetic characteristics of a LSMO/STO thin film. Further, Fig. 1(c) demonstrates that the LSMO thin film was well epitaxially grown on the STO substrate (the zone illuminated by the electron beam is indicated with an orange circle).

All the EELS and EMCD experiments were performed on a FEI Titan 80–300 TEM operating at 300 kV equipped with a postpositional Gatan Tridium system with an energy resolution of 0.7 eV. In our experiments, the convergence angle of the incident beam was less than 0.5 mrad and the diameter of the illuminated area was about 50 nm. The tilt angle was about 9.5° to reach the three-beam diffraction geometry from the [001] zone axis. By tilting the sample further in the perpendicular direction by a small angle of 5 mrad (0.3° with the help of Kikuchi lines), the two-beam diffraction geometries were obtained. The collection angle was about 3.4 mrad. All raw data were processed using Matlab programs, and the signal distributions on the diffraction planes were analyzed with modified automatic term selection algorithm software.[31]

The intensity of the EMCD signal is strongly dependent on dynamical effects, and a proper and optimized dynamical diffraction condition is of significant importance in achieving high a SNR for quantitative measurements. The distributions of dynamical diffraction coefficients under (200) two-beam conditions, (200) three-beam conditions, and (220) two-beam conditions were calculated[30] and are shown in Figs. 2(a), 2(c), and 2(d), respectively. It can be seen that the intensity of dynamical diffraction coefficients under the (200) two-beam condition was slightly better than that under the (220) two-beam condition, while the maximum value under the (200) three-beam condition was only two thirds of that under the (200) two-beam condition.

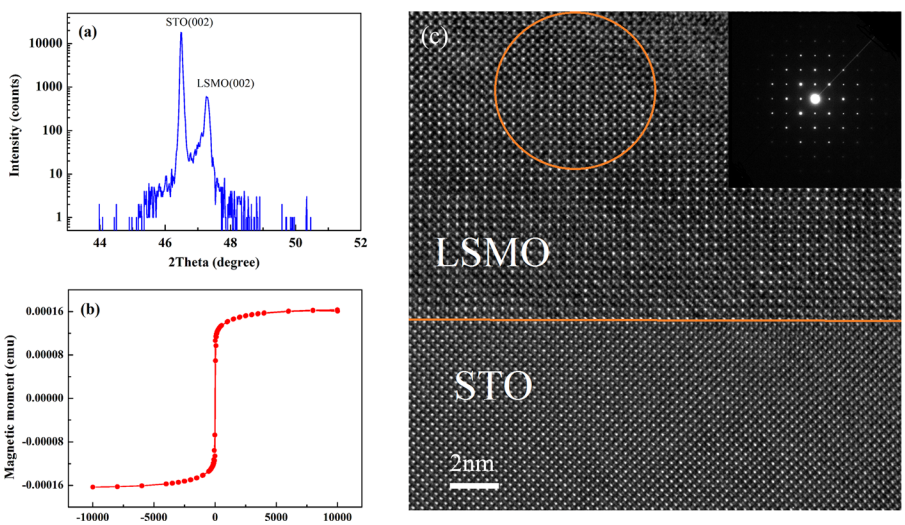

FIG. 1. (a) X-ray diffraction result of LSMO/STO thin film. Both LSMO (002) peak and STO (002) peak are sharp, reflecting good epitaxial growth of the thin film. The LSMO (001) interplanar spacing was 3.844 Å (3.87 Å for the bulk). Panel (b) shows the M-H curve for LSMO/STO thin films. Panel (c) shows the crystal structure near the LSMO/STO interface, and the zone illuminated by electron beam in experiment is circled in orange.

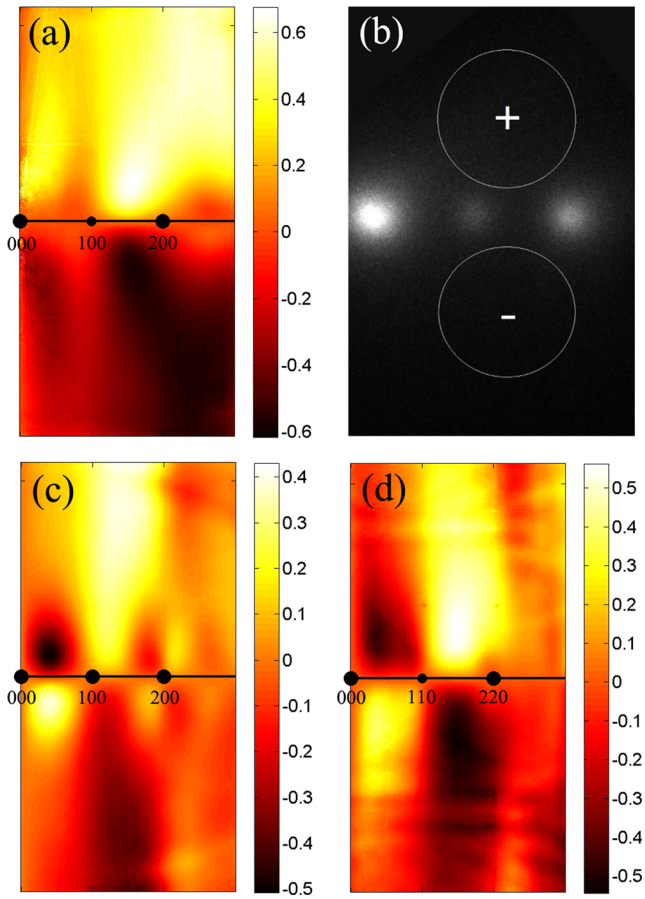

FIG. 2. Intensity simulation of dynamical diffraction coefficients and experimental condition in reciprocal space: (a) simulation of dynamical diffraction coefficients distribution under (200) two-beam diffraction geometry; (b) experimental schematic EELS spectrometer entrance aperture positions; (c) simulation of dynamical diffraction coefficients distribution under (200) three-beam diffraction geometry; and (d) simulation of dynamical diffraction coefficients distribution under (220) two-beam diffraction geometry.

Taking all those factors into consideration, the (200) two-beam diffraction geometry was chosen as the experimental condition in this work in spite of the higher asymmetry of its dynamical coefficients in both the "positive" and "negative" positions, which can be solved by averaging the absolute values.[12] In our experiments, the entrance aperture was located only at the area with strong intensity of the EMCD signals, as shown in Fig. 2(b).

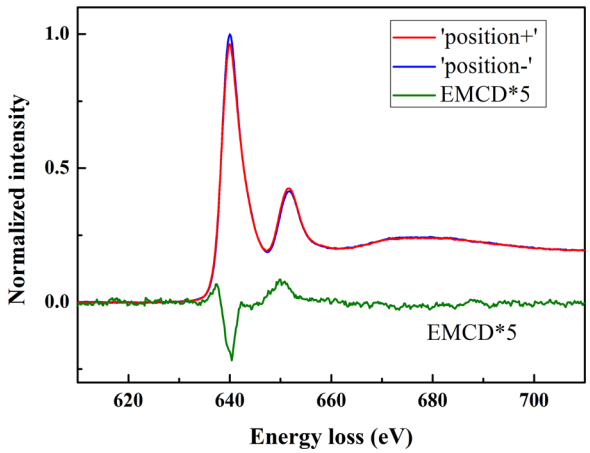

FIG. 3. Normalized EELS in "positive" and "negative" positions and the EMCD signal after calculating the difference.

Though the optimization of dynamical diffraction conditions will help to increase SNR, it is also necessary to optimize the experimental parameters for EELS acquisition. The SNR is proportional to the square root of counts and limited by the count limitations of the CCD; hence, a continuous exposure method was chosen to improve the SNR. In our experiments, each pair of spectra was exposed 10 times successively, each time for 2 s. Then, these spectra were aligned and accumulated to obtain smoother spectra. Furthermore, to deal with a large number of spectra and to eliminate artificial errors, a Matlab program was written to process the acquired spectra under the same criterion, which included the pre-edge background subtraction, deconvolution, post-edge normalization, peak alignment, and deduction of step-functions at the energy-loss edges.

A series of pairs of EELS were acquired and the final results are shown in Fig. 3. It can be seen that the EMCD signal at the L3 edge was opposite to that at the L2 edge. Compared with previously reported EMCD signals, the intensity of signals here was much higher than the background noise, thus improving the credibility of the final quantitative calculation. Since the dynamical diffraction effect has been considered in the simulations, the EMCD signal derived was intrinsic and can be used for quantitative magnetic parameter calculations. By using the sum rules described in the following equation, the magnetic parameters of manganese were derived as shown in Table I:

$$\begin{cases} \dfrac{\int_{L_3}(\sigma_2-\sigma_1)dE - 2\int_{L_2}(\sigma_2-\sigma_1)dE}{\int_{L_3+L_2}(\sigma_2+\sigma_1)dE} = \left(\dfrac{2}{3}\dfrac{\langle S_z\rangle}{N_h} + \dfrac{7}{3}\dfrac{\langle T_z\rangle}{N_h}\right) \approx \dfrac{2}{3}\dfrac{\langle S_z\rangle}{N_h} \\ \dfrac{\int_{L_3+L_2}(\sigma_2-\sigma_1)dE}{\int_{L_3+L_2}(\sigma_2+\sigma_1)dE} = \dfrac{1}{2}\dfrac{\langle L_z\rangle}{N_h}. \end{cases} \tag{1}$$

Here, $\sigma_1 = (\partial^2\sigma/\partial E\partial\Omega)_{pos1}$ and $\sigma_2 = (\partial^2\sigma/\partial E\partial\Omega)_{pos2}$ are the double differential scattering cross sections in the "positive" and "negative" position;[6] $\langle S_z\rangle$, $\langle L_z\rangle$, and $\langle T_z\rangle$ are the expectation values of the spin angular operator, orbital angular operator, and magnetic dipole operator, respectively; and N_h refers to the holes in the d-orbit (taken here to be 6.3 by using the average valence approximation).[32,33]

TABLE I. Magnetic parameters of manganese at the zone distance of about 35 nm from the interface of the LSMO/STO thin film at room temperature.

Magnetic parameters	m_L/m_S	Orbital magnetic moment (μ_B)	Spin magnetic moment (μ_B)
Measured value	(−0.03, 0.01)	(−0.021, 0.007)	0.7 3± 0.26

The errors considered here contained the standard deviation of each single measurement, the uncertainty of the dynamical diffraction dynamical coefficients, the noise of the spectra, and errors in the numerical integration. Our calculation showed that the uncertainty of the orbital-spin ratio mainly originated from the noise of the spectra and errors in the numerical integration, which are larger than the ratio itself because the orbital magnetic moment discussed here is mostly quenched to zero and hard to detect; therefore, giving its lower and upper bound (−0.03, 0.01) is more reasonable in this case. Similarly, the orbital magnetic moment lies in an interval of (−0.021, 0.007) μ_B. However, the uncertainty of the dynamical diffraction dynamical coefficients was the main source of the uncertainty of the spin magnetic moment.

Furthermore, as a proof of the accuracy of our spin magnetic moment value, the macroscopic measurement result was normalized by the film volume; the average magnetic moment in one unit cell is 0.45 μ_B, which seems slightly smaller than the lower bound of our EMCD result ($0.73 \pm 0.26\,\mu_B$); however, this could be explained by the decrease of the magnetic moment near the interface. According to Refs. 22 and 23, the normalized magnetization of LSMO thin films declines as their thickness is decreased, which means that the magnetic moment is lower near the interface. When it comes to our experiment, since the region detected by the electron beam was away from the interface, the spin magnetic moment value of $0.73 \pm 0.26\,\mu_B$ given by the EMCD result is reasonable.

In conclusion, through the enhancement of the EMCD signals by dynamical diffraction effects, the optimization of computational simulation and data processing, we have improved the sensitivity of the EMCD technique with nanoscale spatial resolution for LSMO/STO thin films with weak magnetism. Then, we derived the manganese spin magnetic moment of $0.73 \pm 0.26\,\mu_B$ and limited the ratio of the orbital to spin magnetic moment to within an interval of (−0.03, 0.01). Our results not only present the nanoscale magnetic parameters of LSMO/STO but also demonstrate how the minimum measurement limit of the spin (or orbital) magnetic moment can be achieved via the development of a dynamical diffraction effect assisted EMCD technique; this may promote the use of this technique for nanoscale probing of weak magnetic systems.

This work was financially supported by National 973 Project of China (2015CB654902) and Chinese National Natural Science Foundation (11374174, 51390471, and 51527803). This work made use of the resources of the National Center for Electron Microscopy in Beijing and Tsinghua National Laboratory for Information Science and Technology. We also thank Jan Rusz for providing the modified automatic term selection algorithm software.

[1]J. H. Park, E. Vescovo, H. J. Kim, C. Kwon, R. Ramesh, and T. Venkatesan, Nature **392**, 794 (1998).
[2]H. J. Mao, P. X. Miao, J. Z. Cong, C. Song, B. Cui, J. J. Peng, F. Li, G. Y. Wang, Y. G. Zhao, Y. Sun, L. R. Xiao, and F. Pan, J. Appl. Phys. **116**, 053703 (2014).
[3]A. Urushibara, Y. Moritomo, T. Arima, A. Asamitsu, G. Kido, and Y. Tokura, Phys. Rev. B **51**, 14103 (1995).
[4]H. L. Ju, C. Kwon, Q. Li, R. L. Greene, and T. Venkatesan, Appl. Phys. Lett. **65**, 2108 (1994).
[5]P. Schattschneider, S. Rubino, C. Hébert, J. Rusz, J. Kunes, P. Novák, E. Carlino, M. Fabrizioli, G. Panaccione, and G. Rossi, Nature **441**, 486 (2006).
[6]L. Calmels, F. Houdellier, B. Warot-Fonrose, C. Gatel, M. J. Hÿtch, V. Serin, and E. Snoeck, Phys. Rev. B **76**, 060409(R) (2007).
[7]P. Schattschneider, S. Rubino, C. Hebert, J. Rusz, J. Kunes, P. Novak, E. Carlino, M. Fabrizioli, G. Panaccione, and G. Rossi, Phys. Rev. B **78**, 104413 (2008).
[8]H. Lidbaum, J. Rusz, A. Liebig, B. Hjorvarsson, P. M. Oppeneer, E. Coronel, O. Eriksson, and K. Leifer, Phys. Rev. Lett. **102**, 037201 (2009).
[9]P. Schattschneider, C. Hébert, S. Rubino, M. Stöger-Pollachb, J. Rusz, and P. Novák, Ultramicroscopy **108**, 433 (2008).
[10]J. Salafranca, J. Gazquez, N. Perez, A. Labarta, S. T. Pantelides, S. J. Pennycook, X. Batlle, and M. Varela, Nano Lett. **12**, 2499 (2012).
[11]Z. Q. Wang, X. Y. Zhong, R. Yu, Z. Y. Cheng, and J. Zhu, Nat. Commun. **4**, 1395 (2013).
[12]D. S. Song, Z. Q. Wang, and J. Zhu, Ultramicroscopy **148**, 42 (2015).
[13]D. S. Song, G. Li, J. Cai, and J. Zhu, Sci. Rep. **6**, 18489 (2016).
[14]R. C. Che, C. Y. Lianga, X. He, H. H. Liu, and X. F. Duan, Sci. Technol. Adv. Mater. **12**, 025004 (2011).
[15]B. Warot-Fonrose, C. Gatel, L. Calmels, V. Serin, E. Snoeck, and S. Cherifi, J. Appl. Phys. **107**, 09D301 (2010).
[16]D. S. Song, L. Ma, S. M. Zhou, and J. Zhu, Appl. Phys. Lett. **107**, 042401 (2015).
[17]L. Calmels and J. Rusz, Ultramicroscopy **110**, 1042 (2010).
[18]S. Rubino, P. Schattschneider, M. Stoger-Pollach, C. Hebert, J. Rusz, L. Calmels, B. Warot-Fonrose, F. Houdellier, V. Serin, and P. Novak, J. Mater. Res. **23**, 2582 (2008).
[19]P. Schattschneider, I. Ennen, S. Löffler, M. Stöger-Pollach, and J. Verbeeck, J. Appl. Phys. **107**, 09D311 (2010).
[20]I. Ennen, S. Loffler, C. Kubel, D. Wang, A. Auge, A. Hutten, and P. Schattschneider, J. Magn. Magn. Mater. **324**, 2723 (2012).
[21]X. Fu, B. Warot-Fonrose, R. Arras, D. Demaille, M. Eddrief, V. Etgens, and V. Serin, Appl. Phys. Lett. **107**, 062402 (2015).
[22]A. Tebano, C. Aruta, S. Sanna, P. G. Medaglia, G. Balestrino, A. A. Sidorenko, R. De Renzi, G. Ghiringhelli, L. Braicovich, V. Bisogni, and N. B. Brookes, Phys. Rev. Lett. **100**, 137401 (2008).
[23]F. Sandiumenge, J. Santiso, L. Balcells, Z. Konstantinovic, J. Roqueta, A. Pomar, J. P. Espinos, and B. Martinez, Phys. Rev. Lett. **110**, 107206 (2013).
[24]J. S. Lee, D. A. Arena, P. Yu, C. S. Nelson, R. Fan, C. J. Kinane, S. Langridge, M. D. Rossell, R. Ramesh, and C.-C. Kao, Phys. Rev. Lett. **105**, 257204 (2010).
[25]J. J. Kavich, M. P. Warusawithana, J. W. Freeland, P. Ryan, X. Zhai, R. H. Kodama, and J. N. Eckstein, Phys. Rev. B **76**, 014410 (2007).
[26]M. Hujiben, L. W. Martin, Y.-H. Chu, M. B. Holcomb, P. Yu, G. Rijnders, D. H. A. Blank, and R. Ramesh, Phys. Rev. B **78**, 094413 (2008).
[27]J. O'Donnell, A. E. Andrus, S. Oh, E. V. Colla, and J. N. Eckstein, Appl. Phys. Lett. **76**, 1914 (2000).
[28]H. Boschker, J. Kautz, E. P. Houwman, W. Siemons, D. H. A. Blank, M. Huijben, G. Koster, A. Vailionis, and G. Rijnders, Phys. Rev. Lett. **109**, 157207 (2012).
[29]C. G. Duan, S. S. Jaswal, and E. Y. Tsymbal, Phys. Rev. Lett. **97**, 047201 (2006).
[30]See supplementary material at http://dx.doi.org/10.1063/1.4954168 for details of deposition of LSMO/STO thin films and simulation of EMCD signals.
[31]J. Rusz, S. Muto, and K. Tatsumi, Ultramicroscopy **125**, 81 (2013).
[32]P. Carra, B. T. Thole, M. Altarelli, and X. Wang, Phys. Rev. Lett. **70**, 694 (1993).
[33]W. L. O'Brien and B. P. Tonner, Phys. Rev. B **50**, 12672 (1994).